

Event-based RGB-D sensing with structured light

Seyed Ehsan Marjani Bajestani
Polytechnique Montreal
ehsan.marjani@polymtl.ca

Giovanni Beltrame
Polytechnique Montreal
giovanni.beltrame@polymtl.ca

Abstract—Event-based cameras (ECs) are bio-inspired sensors that asynchronously report brightness changes for each pixel. Due to their high dynamic range, pixel bandwidth, temporal resolution, low power consumption, and computational simplicity, they are beneficial for vision-based projects in challenging lighting conditions and they can detect fast movements with their microsecond response time. The first generation of ECs are monochrome, but color data is very useful and sometimes essential for certain vision-based applications. The latest technology enables manufacturers to build color ECs, trading off the size of the sensor and substantially reducing the resolution compared to monochrome models, despite having the same bandwidth. In addition, ECs only detect changes in light and do not show static or slowly moving objects. We introduce a method to detect full RGB events using a monochrome EC aided by a structured light projector. The projector emits rapidly changing RGB patterns of light beams on the scene, the reflection of which is captured by the EC. We combine the benefits of ECs and projection-based techniques and allow depth and color detection of static or moving objects with a commercial TI LightCrafter 4500 projector and a monocular monochrome EC, paving the way for frameless RGB-D sensing applications.

Index Terms—event-based camera, monochrome, color reconstruction, color detection, colorization, structured light

I. INTRODUCTION

Event-based cameras (ECs) report brightness changes asynchronously for each pixel, a behavior inspired by the human eye [1]. When the brightness changes over a certain threshold for a pixel, the camera generates an event containing the coordinates of the pixel (x,y) , a timestamp, and the polarity of the event (i.e. increasing or decreasing). Although ECs do not capture full images, they can detect movement thousands of times faster than standard frame-based sensors, and since they do not have an external shutter cycle, their output is event-driven and frameless, resulting in very low latency, power consumption, and bandwidth demands.

Due to their advantages, ECs have been used in various computer vision applications such as fast movement detection and tracking [2]–[4], optical flow, pose tracking and visual-inertial odometry [5], [6], Simultaneous Localization And Mapping (SLAM) [7], [8], pattern recognition [9], depth estimation and stereo vision [10]–[12], and many more.

In computer vision, color information has an important role [13] and could be essential to many tasks such as segmentation and recognition [14]. The first generation of ECs are monochromatic, with color ECs only recently becoming available [15]–[18]. However, due to limitations in terms of sensor size, color ECs have lower resolution than mono ECs because they need to use color filters.

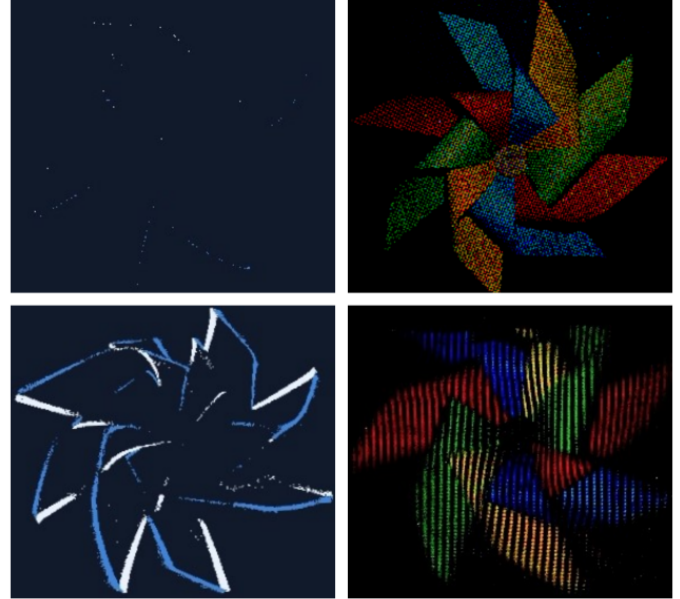


Fig. 1. Color detection of a stable (top row) and spinning (bottom row) colorful paper pinwheel. Left column: monochrome events without structured light. Right column: colorful image reconstructed aided by structured light with two patterns and equivalent speeds of 30 fps (top) and 150 fps (bottom).

It is worth noting that ECs report pixel brightness changes, meaning that an EC will not report anything when the camera (and/or the object in its field of view) is static or slowly moving (Fig. 1, top left), which can be critical in some cases (e.g. for a slow-moving robot). To overcome this issue, one could use an external active device such as a laser, a flashing LED, or a light projector to generate events in static and almost static situations. This external active lighting system could also be used to detect depth by projecting detectable patterns called Structured Light (SL) [19]–[22].

We present a method to add color and depth to a monocular, monochrome event-based camera while maintaining fast response time and resolution. We use a Digital Light Processing (DLP) projector that emits patterns of lights that we call Active Structured Light (ASL) on a scene, the reflection of which is captured by the EC which in turn generates events tagged with the color and depth of the scene. It is worth noting that our ASL method could also be used with color ECs, allowing the detection of static scenes. By dynamically adjusting the projection, we have color data when needed,

managing the overall bandwidth of the system. For example, we can use the full resolution of the camera to detect static color scenes, or use more sparse patterns for fast moving objects. Projecting patterns also allows triangulation-based measurements to create a colorful 3D point cloud of the scene.

Overall, we present 5 contributions:

- 1) the generation of colorful events from a monochrome EC for various speeds of movement;
- 2) a higher-resolution version of a color EC using a monochrome EC;
- 3) we allow the detection of static objects and scenes;
- 4) we optimize the bandwidth usage of the EC by detecting the color when and where it is needed;
- 5) we use patterns that allow event-based depth measurement, ultimately generating colorful point clouds.

In this work we focused on visual light wavelength (emitted by the LED projector) and materials that are not in the category of fluorescence and they do not change the wavelength of the light. We validated our approach in different dynamic conditions: Fig. 2 shows the experimental setup with a DLP projector¹ and a Prophesee evaluation kit². With this setup, we achieved full color detection at an equivalent rate of 1400 frames per second (fps) (note that the camera is frameless, we use fps just for the purpose of comparison). Fig. 2 also shows the color detection of a static printed color wheel.

The rest of the paper is as follows: Section II presents related work; Section III describes our method for color detection; Section IV details the results of our method in several conditions; and finally, Section V draws some concluding remarks and outlines possible future work.



Fig. 2. Left: The experimental setup with a DLP LightCrafter 4500 Evaluation Module and a Prophesee evaluation kit (Gen3-VGA). Middle: Printed color wheel with the logo of the MIST Lab., captured by a frame-based high-resolution camera. Right: Colorful image reconstructed by proposed method captured by monochrome EC aided by SL.

II. RELATED WORK

Digital color cameras use various Color Filter Array (CFA) or Color Filter Mosaic (CFM) on their sensors to detect different colors for each pixel, and among them, the Bayer array filter [23] is the most common CFA [24]. Using a

CFA, the resolution of a monochrome photosensor decreases dramatically, since the size of the CFA could be between 4 to 36 pixels or even bigger based on its design [25]. This means that, even with the smallest CFA, to have a color pixel we need several monochrome pixels, which decreases the available resolution (e.g. 4 times with a CFA size of 2×2 pixels).

Colorization is the process to generate a color image based on a monochrome sensor or grayscale image without loss of resolution. Colorization requires either external data about the image colors, user interaction, or a trained neural network embedding the knowledge of the colors on the scene, and can be a time-consuming and expensive task [26]. Levin et al. [26] introduced a method that needs a few initial inputs from a user to generate a full color image and keeps tracking the color on upcoming frames in a video. Zhang et al. [27] introduce a fully automatic colorization approach based on a convolutional neural network (CNN) that can change a grayscale image into a near-real colorful image. Their method successfully deceived 32% of human participants in distinguishing the generated image compared with the ground truth image. In contrast to these colorization approaches, our method does not need initial input data to get color out of a monochrome camera and it can provide realistic color information faster than CNN models.

Another approach to generate color data without quality loss on a monochrome image is to use separate cameras: the monochrome sensor takes a more detailed and higher contrast image, while a lower resolution RGB camera adds color information. This combination of an RGB camera with a monochrome sensor is very common, but the image fusion, colorization, or the color transfer process are still a challenge [28].

Event-based cameras have introduced a new field of imaging systems. Due to their advantages compared to standard cameras, many scientists investigated ways to generate and reconstruct images from events to use in frame-based computer vision algorithms. A monochrome EC has been used in many image reconstruction works [29]–[34]. Also, a dual-cameras consisting of a standard frame-based camera and an EC can produce a deblurred high frame rate (HFR) and high dynamic range (HDR) video [35].

By combining three ECs using dichroic filters Marcireau et al. [14] introduced a prototype to capture a stream of events in RGB separate channels for color segmentation. This allowed them to keep the resolution of the monochrome EC, however, the required bandwidth increased by three times.

With the introduction of color event-based cameras [17], some research focused on the reconstruction of images and videos based on color events [36]–[38]. Scheerlinck *et al.* [39] presented a dataset for color ECs. They also compared the output quality of some image reconstruction methods such as [29]–[31] in color.

As digital color cameras, current color ECs also use CFA to generate color events, which reduces their output resolution. Compared to the method presented by Marcireau et al. [14], despite having a lower resolution, the CFA-based color ECs

¹LightCrafter 4500 Evaluation Module

²Gen3-VGA

need lower bandwidth. Our method reconstructs color data when it is needed, which controls the bandwidth of the system.

III. MONOCHROME TO COLOR

Compared to frame-based cameras, ECs are faster sensors, however, since they report nothing in a static situation or with slowly moving objects, they require an additional sensor to provide visual perception in these situations. We use an external event generator, namely a DLP projector. By emitting a pattern of light on objects in the scene, not only we can detect their color, but we are also able to detect depth, which makes event-based RGB-D sensing possible. Moreover, since ECs have a high dynamic range sensor, there is no need to have a high-power light projector to see dark environments.

There are many standard color formats for digital color descriptions (additive or subtractive), such as CMY (cyan, magenta, yellow), or with black CMYK, RYB (red, yellow, blue), RGB (red, green, blue) or with white RGBW and etc. Selecting the color space could depend on the application and the color range of the desired objects in the environment. Without loss of generality, we select the RGB color space which is more common in vision applications.

We use the EC to measure the amount of reflection of the emitted light on an object. To measure the color, we project three different wavelengths (structured light in red, green, and blue) on the environment and measure the amount of reflected light captured by the EC. During each pattern exposure time, the received events are gathered in an appropriate color channel on the initial frame. Fig. 3 shows the procedure for color detection.

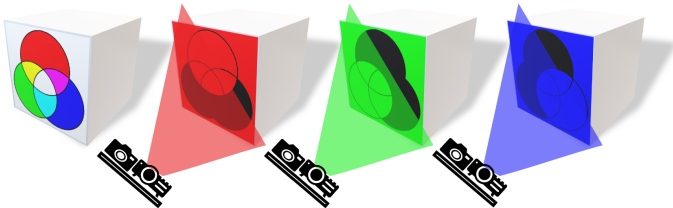


Fig. 3. The procedure of detecting color with a monochrome event-based camera aided by structured light. From left to right: The colorful object, SL pattern projected in red, green, and blue by the DLP projector and collecting the events by EC.

To synchronize the DLP projector with the EC, we connect the trigger pins of the camera to the projector. By changing the pattern color, the DLP sends a pulse to the camera which identifies the incoming events as belonging to the appropriate color channel. Fig. 4 depicts the output of the color detection of a printed RGB color wheel separated in each color channel. The bottom frame of the Fig. 4 shows that the printed color wheel does not have pure green $(0, 255, 0)$ and blue $(0, 0, 255)$ colors in 24 bit RGB format. For example, in the red light channel (bottom left), the green circle also reflected some light (although less than the red circle) and as a result, it appears gray.

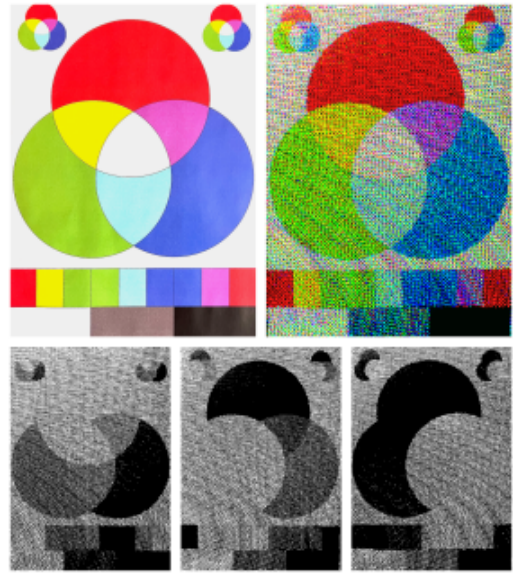


Fig. 4. Color detection of a printed color wheel. Top left captured by frame-based high-resolution camera, top right is colorful image reconstructed by proposed method, captured by a VGA monochrome EC aided by SL. Bottom from left to right are collected event-frames for each color light (red, green and blue) by monochrome EC.

A. Color detection speed limits

One of the main advantages of the ECs is their response time which is in the range of microseconds. However, with the introduced method, we need to gather events of each color separately, limiting the speed of color detection to the maximum speed of pattern switching of the DLP projector. With the LightCrafter 4500 Evaluation Module, we are able to detect color with an equivalent frame rate up to 1400 fps due to its high frequency (4225 Hz¹). However, assuming that the color of the object is not changing, we could still use the other methods to track the object only based on the high speed stream of events [3], [4] and use the color detection method for a short period of time. Fig. 5 shows the output of the color detection of a spinning colorful paper pinwheel reconstructed at different frame rates.

B. Advantages over monochrome frame-based cameras

Monochrome or grayscale cameras have been used in vision-based applications that do not need color information. As mentioned in Section II, the combination of a monochrome camera and a color camera could be challenging for image fusion, colorization, or the color transfer process [28]. A dual-camera consisting of a frame-based camera and an EC can produce a deblurred high frame rate (HFR) and high dynamic range (HDR) video [35]. However, by adding a second camera the required bandwidth increases at the same time. Our method allows us to benefit from ECs' features and detect/update the color information for a given period of time. Moreover, the

¹Switching rate for preloaded 1 Bit depth pattern of the LightCrafter 4500 Evaluation Module

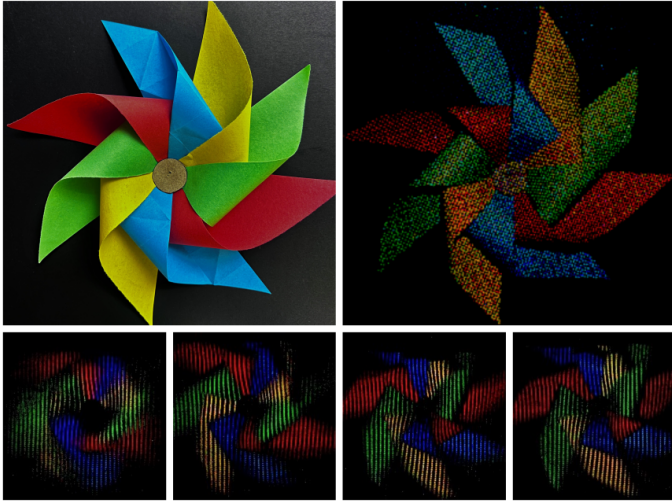


Fig. 5. Color detection of a spinning colorful paper pinwheel reconstructed at different frame rates. Top row (static) left: captured by frame-based high resolution camera, right: colorful image reconstructed by proposed method captured by monochrome EC. Bottom row (spinning pinwheel) reconstructed at, from left to right, 30, 100, 120 and 150 fps.

camera-projector combination enables depth measurement and makes the feature detection and matching easier (compared to stereo cameras) [19]–[22].

C. Advantages over color event-based cameras

As mentioned in Section II, digital cameras often use CFA to detect color. For instance, the Color-DAVIS346 [16] is one of the most recent color EC that uses an RGBG Bayer pattern with an output resolution of 346×260 pixels. This kind of camera is reporting the stream of events in 3 or 4 different channels, which increase the need for bandwidth. Higher bandwidth requirements can cause bus saturation (as described in Section IV). In addition, despite increasing the bandwidth needs and decreasing the resolution, color ECs cannot detect the environment when the camera or object is static or moving very slowly. Our method is useful to efficiently use the bandwidth by detecting the color only when and where it is needed. Moreover, our method also gathers information from the environment from an initially static robot or camera, meaning there is no need to have mechanical parts to move the camera and receive events, which makes the system more reliable. Further, since a high-resolution EC could be subject to more noise in a dark environment compared with a low-resolution EC [40], our method could still get the benefits of the high-resolution monochrome EC in a dark environment.

D. White balance and color correction

White balance and color correction can make the captured image close to its natural color. White balance can be adjusted before or after capturing the image. Generating white light with the DLP projector can change the image white balance, because the color temperature of a light source or the warmth/coolness of the white light can change the white

balance directly. The DLP projector has three different LED colors: red, green, and blue. Generating LED-based white light could be challenging with wideband wavelength RGB LEDs [41]–[43]. Since the DLP projector has narrowband LEDs, changing the white balance can be done relatively easily by changing the current of each LED separately.

Lighting model: If we consider the DLP projector as a point-sized light source, we can model the lighting with the Lambertian shading model which is one of the simplest bidirectional reflectance distribution functions (BRDF) and an appropriate approximation to many real-world material surfaces [44]. In the Lambertian shading model, R, G, B values of the resulting pixel are independent of the angle that the viewing ray hits the surface:

$$W = S_{ref} S_{pow} \max(0, n \cdot b), \quad (1)$$

where W is the combination of (R, G, B) values for a desired pixel, and S_{ref} is the spectral reflectance of the material, S_{pow} represents the spectral power distribution of the projector (as the light source), n is the outward surface normal (of the object) and b is the light beam vector which is from the surface intersection point to the projector. The dot product of these two unit vectors gives the amount of attenuation based on the angle between the surface to the projector. The \max function is used to prevent a condition where $n \cdot b < 0$, because the projector would be behind the object in this case. This model could be divided for each color, for example the model for red light is:

$$R = S_{ref_R} S_{pow_R} \max(0, n \cdot b) \quad (2)$$

To generate white light in an ideal situation, we consider that each color has the same power distribution and $S_{pow_R} = S_{pow_G} = S_{pow_B}$. And for a white or gray surface we would have $S_{ref_R} = S_{ref_G} = S_{ref_B}$. As a result, by controlling the current of each LED (S_{pow}) we can have balanced white light.

We can use a gray card, a color wheel, or a Macbeth color chart/color checker to calibrate our system. We used a printed Macbeth color chart to do the calibration, and Fig. 6 shows the output of the color detection with the proposed method with and without white balance calibration.

Absolute error: To check the quality of the reconstructed image, we need to have a base image and specify an error calculation method. We consider the captured image by a frame-based high-resolution camera as the base image (Ground Truth or GT) in Fig. 6. To calculate the absolute error, we compared the histogram of two images in Hue Saturation Value (HSV) format based on the correlation metric¹:

$$c = d(H_o, H_b) = \frac{\sum_I (H_o(I) - \bar{H}_o)(H_b(I) - \bar{H}_b)}{\sqrt{\sum_I (H_o(I) - \bar{H}_o)^2 \sum_I (H_b(I) - \bar{H}_b)^2}}, \quad (3)$$

where

¹The OpenCV histogram comparison correlation method.

$$\bar{H}_k = \frac{1}{N} \sum_J H_k(J), \quad (4)$$

and N is the total number of histogram bins, which in our case is 256 (8 bit in each color channel). The H_o and H_b are respectively histogram of the output image and the baseline image with a Histogram Correlation (HC) between 0 and 1. The HC between the base image (left) and each reconstructed image is respectively 0.22 and 0.76 for the reconstructed image without white balance (middle) and with white balance (right) in Fig. 6. Moreover, to check the difference between each pixel in the reconstructed image and the GT, and calculate the absolute error, we calculated the root mean square error (RMSE) separately for each channel. As an example, the RMSE for the red channel is:

$$RMSE_r = \sqrt{\frac{\sum_N (p_{o_r} - p_{b_r})^2}{N}}, \quad (5)$$

where p_{o_r} and p_{b_r} are respectively the pixel value in the red channel of the output frame and the baseline frame. N is the total number of pixels, i.e. $640 \times 480 = 307200$. Table I shows the quality of the color detection for each image in Fig. 6 compared to the GT image. Table I also shows that, after manual white balance tuning, all three channels had 12% better RMSE on average. To have a more realistic color detection, an online white balance calibration could be helpful in minimizing the average RMSE if needed. To check the quality of each image we also calculated their Peak Signal-to-Noise Ratio (PSNR), also shown in Table I.

TABLE I
COLOR DETECTION QUALITY TABLE COMPARED TO THE GROUND TRUTH (GT) FRAME

	GT	No WB	WB
$RMSE_{red}$	0	83.89	83.65
$RMSE_{green}$	0	87.79	71.16
$RMSE_{blue}$	0	92.76	76.97
$RMSE$	0	88.15	77.26
$PSNR$	0 dB	9.88 dB	8.82 dB
Histogram Correlation (HC)	1	0.22	0.76

Another way to do the color correction is to capture the image with a white channel by RGBW color spaces and perform the correction on four channels similar to RGBW CFA-equipped sensors [45]. This comes at the cost of adding a 4th color light to the SL, adding at least 33% to the length of the capture time.

IV. ASL: ADAPTIVE STRUCTURED LIGHT

High-resolution ECs have a higher event rate and need more bandwidth compared to low-resolution ECs, but each EC has a limited data rate (finite bandwidth) on the output interface or bus. If the data rate or the number of events exceeds the limit, bus saturation could happen [1], [40]. Filtering [46] or online event-rate control [47] can mitigate this issue. When using an external event generator such as the DLP projector which emits SL on the scene, controlling the event rate is

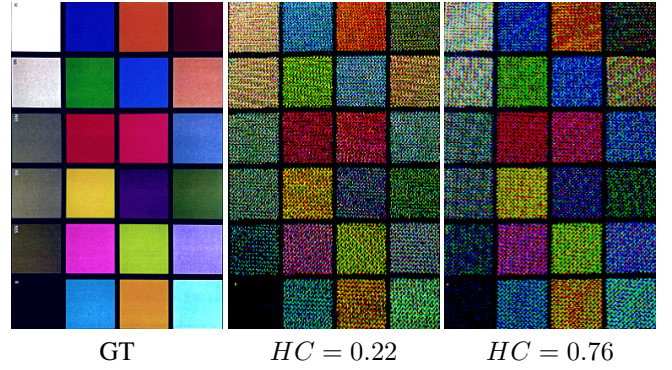


Fig. 6. Color detection of printed Macbeth color chart. Image captured by a frame-based high-resolution camera (left), the colorful image reconstructed by the proposed method captured by monochrome EC, without (middle) and with (right) white balance.

even more important. One method to control the event rate when using a projector is to define a region of interest (ROI) and project the pattern only where it is needed. Muglikar et al. [21] used one EC camera to detect the ROI (generally the area of the image frame that has more events due to the movement) and then projected the SL on that area followed by detecting the depth with a second EC. Instead of adding a second EC to the system, we introduced ASL to control the event-rate. Fig. 7 shows different patterns of the SL which change based on the number of received events. As expected, there is a trade-off between having high-resolution (dense) and high-speed (sparse) color detection. The generated SL patterns are:

- 1) Dot pattern
- 2) Multiple-lines pattern
- 3) Moving-line pattern
- 4) Solid pattern

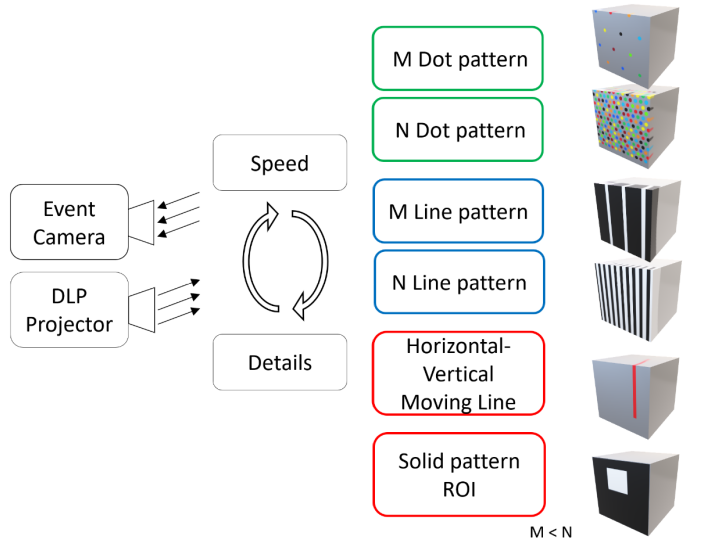


Fig. 7. Different types of SL patterns have been used to control the event rate by Adaptive Structured Light.

In static conditions, ASL could also be used with a color EC and white light. However, it should be noted that color ECs need more bandwidth compared to monochrome ECs with the same resolution.

Bandwidth control: By frequently projecting SL into the scene, we receive events caused by the SL alongside the events caused by the movement of objects or the camera. We want to control the biases of the camera to prevent bus saturation, but we do not want to lose data by excessively decreasing the camera sensitivity. In general, the total number of events should be less than the maximum bandwidth of the EC:

$$\text{Max.Bandwidth} < \text{events}_{SL} + \text{events}_M, \quad (6)$$

where events_M is the number of events caused by the movement of the EC or any object in the scene (i.e., any other events that have not emerged due to the SL). events_{SL} is the number of events caused by the SL, and we can control it by changing the pattern and the power of the LED projector.

events_{SL} is not only linked to the color of the object (and its reflectivity/fluorescence percentage, which we do not investigate in this paper), but also it is related to the distance of the camera-projector from the object. Increasing the distance, the spectral power distribution decreases because of the reduction in power density. Unfortunately, there is no information available concerning the variation of power density changes with distance for each LED of the DLP projector. Modelling the DLP projector power density could be useful, but it is out of the scope of this paper. In this work, we make the simplifying assumption that the power density of all LEDs is the same. As a result, to control events_{SL} at a same distance, we need to control S_{pow} from (1).

Considering a one-bit pattern, we can control S_{pow} by changing the pattern (changing the number of white pixels in a black and white frame), instead of changing the current of the LEDs. We call the number of white pixels per frame as the coverage percentage (CP), with each pattern type having a different CP. To additionally simplify the problem, we assume that the DLP and the EC are close and we can consider the CP on the DLP frame plane despite the fact that, depending on the relative pose of the camera to the projector, the CP could be different on the camera frame plane.

Fig. 8 shows the colorful board that we use in our experiments, placed 160cm from the camera-projector.

A. Dot pattern

Dot grid and circle patterns are one of the simplest patterns to detect the local depth from SL [48] or even calibrating the camera when it is out of focus [49]. Changing the number of dots (feature points) or their distance affects the depth resolution. However, more feature points lead to additional processing time as well as generating more events, which can lead to bus saturation in ECs. By changing the number of dots dynamically based on the event rate, we are able to control the trade-off between the speed of scanning and the amount of detail. Fig. 7's top two rows show the proposed ASL with dot-grid patterns where M and N ($M < N$) are the number



Fig. 8. A colorful board used to test ASL. The board was placed at a distance of 160 cm from the camera projector.

of dots on each grid. Fig. 9 shows three different dot patterns with different CPs. The top row is generated with a temporal window size of 2.5ms (equivalent to 400fps). Similarly, the second row has a window of 4.34ms or 230fps, and the bottom row for 7.14ms or 140fps. The leftmost column of Fig. 9 is a ground truth (GT) frame generated with a one-second temporal window; the middle column is an example frame among the 430 frame samples. We compare each frame pixel by pixel with the GT frame to compute the $RMSE$ for each channel, shown in the rightmost column.

B. Multiple-lines pattern

Since dot-grid patterns are leading to a sparse image, to generate a dense image, line patterns are preferred in low-speed 3D scanning and multi-shot 3D measurement methods. Sequential projection techniques mostly use strip lines [50]. Since the DLP projector can quickly switch (4225 Hz) between patterns, it is possible to generate a dense graph for some region of the object by projecting lines and measuring the depth with triangulation. Although for the spaces between lines we do not have measurements, increasing the number of lines generates more features and it covers a larger area. Similarly to the dot-grid pattern, increasing the number of lines or dots increases the scanning processing time and event rate, and speed and detail must be traded off. The third and fourth rows from top in Fig. 7, show the proposed ASL with the line patterns where M and N ($M < N$) are the number of lines in each pattern.

C. Moving-line pattern

To have a full dense scanning in 3D, a line pattern is very common [19], [20], [22]. We propose to use a moving line pattern (horizontal or vertical depending on the offset between the camera and the projector), when the event rate is lower than the bandwidth limits, providing dense scanning, as shown in the fifth row from top in Fig. 7. Fig. 11 shows the colorful board scanned by a moving-line pattern.

D. Solid pattern

Whenever the 3D scanning is performed, or when we need the color information only for a specific area (the region

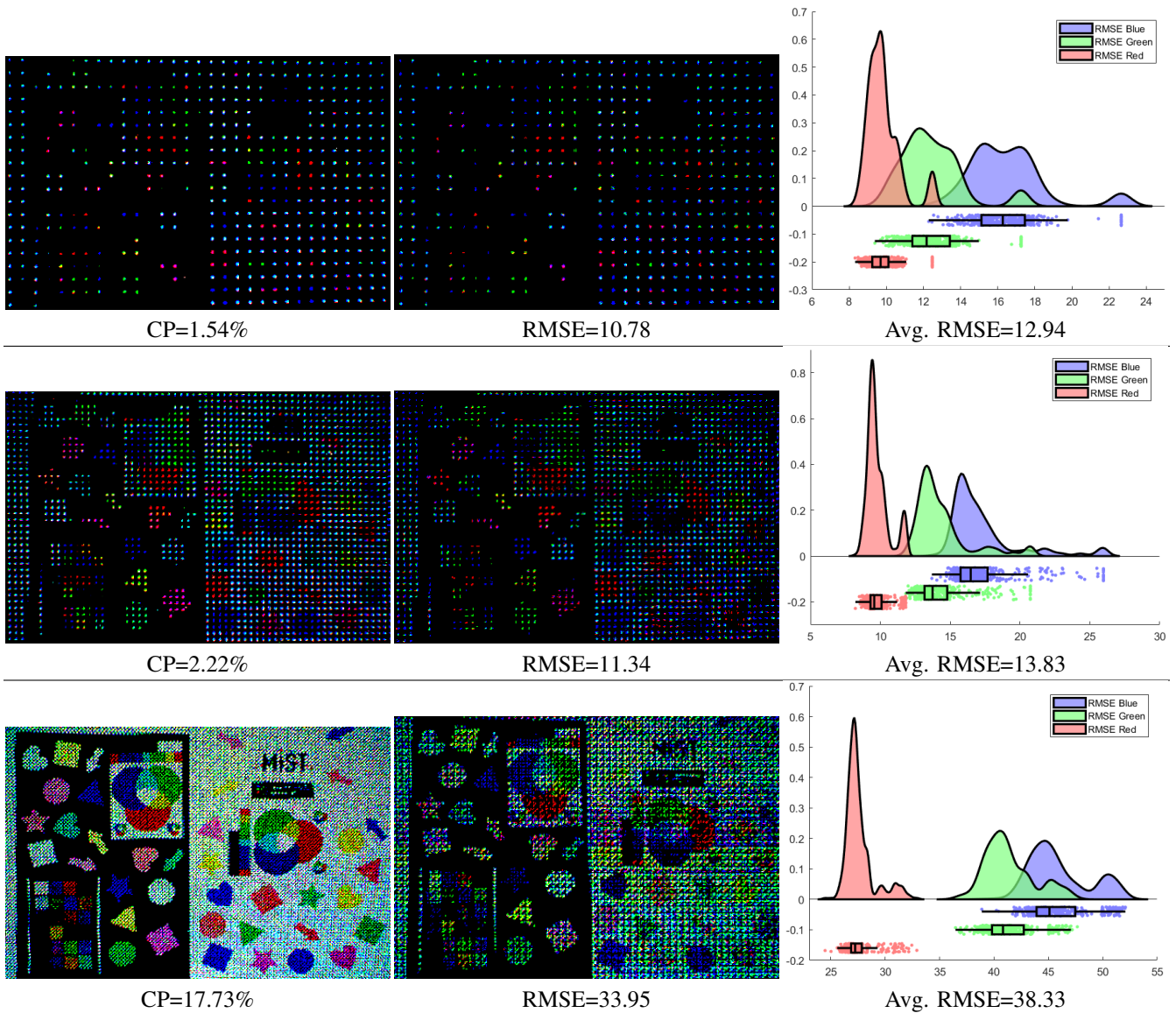


Fig. 9. The colorful board is scanned aided by dot patterns with different CPs. The temporal window size from top to bottom rows are respectively 2.5ms, 4.34ms, and 7.14ms.

of interest), we can use the ROI mode. As described in Section IV, Muglikar et al. [21] defined an ROI dynamically based on the situation of the scene, then scanned that area with more laser points. The bottom row of Fig. 7, indicates the proposed ASL with the solid pattern for the ROI mode. Fig. 12 shows the colorful board scanned by solid pattern for a ROI that is the area of the MIST and Polytechnique Montreal logos.

To compare different pattern and speed of scanning, we projected patterns with various CPs onto the colorful board. Fig. 13 shows the trade-off between details, speed, and the quality of the reconstructed colorful image. It shows that to have a more detailed image, we need to spend more time switching patterns to cover more area. Also, for high speed scanning, a sparse pattern (lower CP with fewer details) is

needed. It is worth noting that a sparse pattern does not decrease the quality of the color detection even with high speed sampling. Fig. 13, has been generated by using around 24000 frames.

V. CONCLUSIONS

We present a method to add color and depth to a monocular, monochrome event-based camera while maintaining fast response time and resolution. Our method reconstructs colorful events and frames using a monochrome EC aided by adaptive structured light (ASL). By dynamically adjusting the projection, we have color data when needed, managing the overall bandwidth of the system. We achieved the color detection speed equivalent of 1400 fps with a Texas Instrument's DLP LightCrafter 4500 projector. Our method could be used

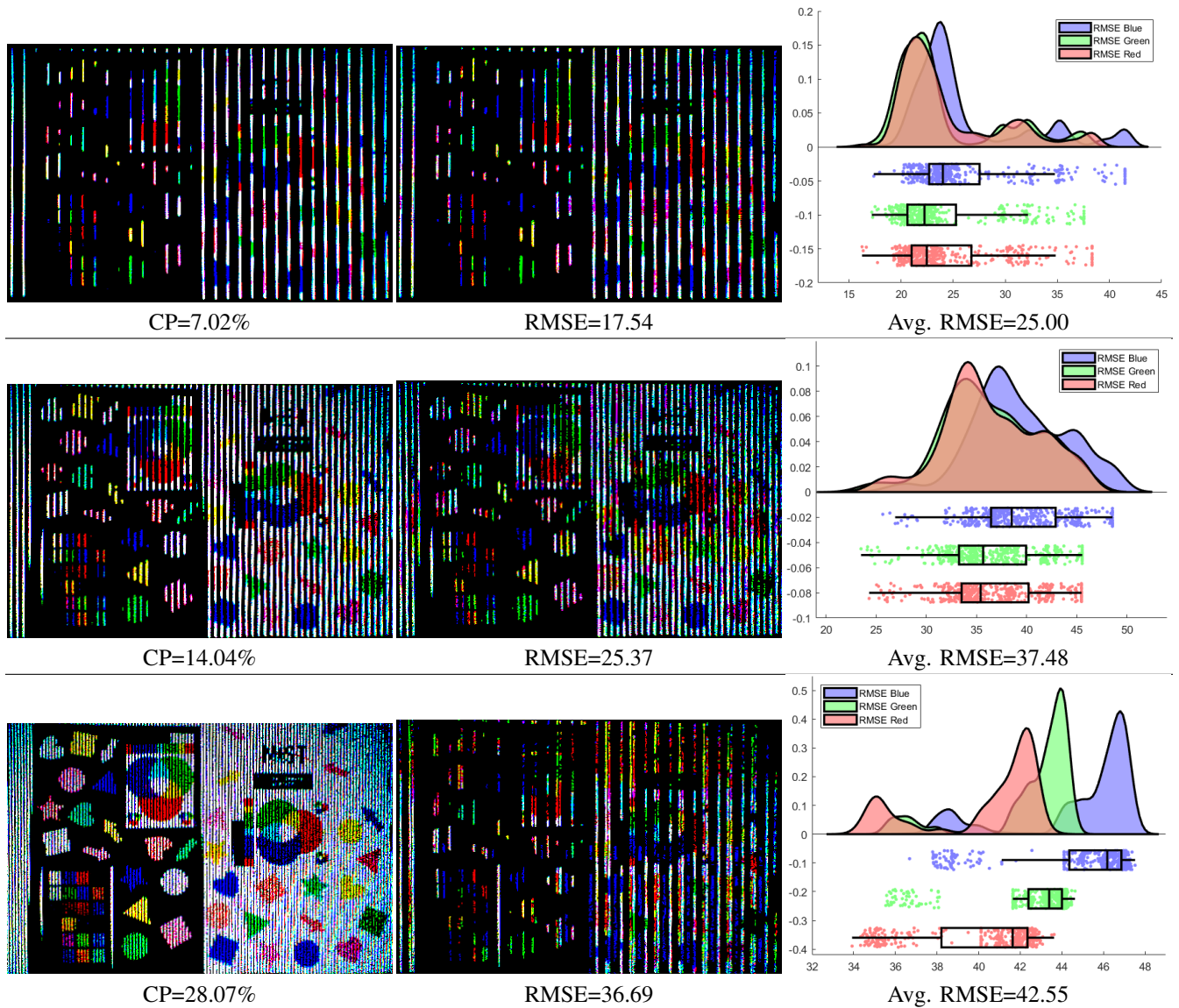


Fig. 10. The colorful board scanned by line patterns with different CPs. The temporal window size for the top row is 6.67ms and for the middle and the bottom rows is 7.14ms.

in event-based depth measurement and perception projects. Advantages of ECs, makes the colorful depth detection much faster than RGBD cameras.

Although the color detection is related to the lighting conditions and material properties at the intersection point (object surface), the scope of this work was the color detection on common materials that are generally matte and not too shiny (with high reflection) or fluorescence. Some materials can interact with light: they can be absorbing, scattering or emitting light [51]. In this work we focused on visual light wavelength (emitted by the LED projector) and materials that are not in the category of fluorescence and they do not change the wavelength of the light. However, the use of the event-based camera with a different type of light source and materials could be investigated in future works. Also, without

considering color detection, static reflective materials can be scanned more effectively with ECs when compared to the other depth measurement devices [20]. To detect the color of these kind of materials, a Blinn-Phong shading model [52] could be considered in future works.

REFERENCES

- [1] G. Gallego, T. Delbruck, G. Orchard, C. Bartolozzi, B. Taba, A. Censi, S. Leutenegger, A. Davison, J. Conradt, K. Daniilidis *et al.*, "Event-based vision: A survey," *IEEE Transactions on Pattern Analysis and Machine Intelligence*, 2020. [Online]. Available: <https://ieeexplore.ieee.org/document/9138762>
- [2] J. Barrios-Avilés, T. Iakymchuk, J. Samaniego, L. D. Medus, and A. Rosado-Muñoz, "Movement detection with event-based cameras: Comparison with frame-based cameras in robot object tracking using powerlink communication," *Electronics*, vol. 7, no. 11, p. 304, 2018. [Online]. Available: <https://www.mdpi.com/2079-9292/7/11/304>



Fig. 11. The colorful board scanned by moving-line pattern.



Fig. 12. The colorful board scanned with a solid pattern for specific ROI. Note that the board was placed 160cm far from the monochrome EC that has a VGA resolution.

- [3] A. Mitrokhin, C. Fermüller, C. Parameshwara, and Y. Aloimonos, "Event-based moving object detection and tracking," in *2018 IEEE/RSJ International Conference on Intelligent Robots and Systems (IROS)*. IEEE, 2018, pp. 1–9. [Online]. Available: <https://ieeexplore.ieee.org/document/8593805>
- [4] I. Alzugaray and M. Chli, "Asynchronous corner detection and tracking for event cameras in real time," *IEEE Robotics and Automation Letters*, vol. 3, no. 4, pp. 3177–3184, 2018. [Online]. Available: <https://ieeexplore.ieee.org/document/8392795>
- [5] A. Zihao Zhu, N. Atanasov, and K. Daniilidis, "Event-based visual inertial odometry," in *Proceedings of the IEEE Conference on Computer Vision and Pattern Recognition*, 2017, pp. 5391–5399. [Online]. Available: https://openaccess.thecvf.com/content_cvpr_2017/html/Zhu_Event-Based_Visual_Inertial_CVPR_2017_paper.html
- [6] E. Mueggler, G. Gallego, H. Rebecq, and D. Scaramuzza, "Continuous-time visual-inertial odometry for event cameras," *IEEE Transactions on Robotics*, vol. 34, no. 6, pp. 1425–1440, 2018. [Online]. Available: <https://ieeexplore.ieee.org/document/8432102>
- [7] H. Rebecq, T. Horstschäfer, G. Gallego, and D. Scaramuzza, "EVO: A geometric approach to event-based 6-dof parallel tracking and mapping in real time," *IEEE Robotics and Automation Letters*, vol. 2, no. 2, pp. 593–600, 2017. [Online]. Available: <https://ieeexplore.ieee.org/document/7797445>
- [8] C. Reinbacher, G. Munda, and T. Pock, "Real-time panoramic tracking for event cameras," in *2017 IEEE International Conference on Computational Photography (ICCP)*. IEEE, 2017, pp. 1–9. [Online]. Available: <https://ieeexplore.ieee.org/document/7951488>
- [9] A. Sironi, M. Brambilla, N. Bourdis, X. Lagorce, and R. Benosman, "Hats: Histograms of averaged time surfaces for robust event-based object classification," in *Proceedings of the IEEE Conference on Computer Vision and Pattern Recognition*, 2018, pp. 1731–1740. [Online]. Available: https://openaccess.thecvf.com/content_cvpr_2018/html/Sironi_HATS_Histograms_of_CVPR_2018_paper.html
- [10] Y. Zhou, G. Gallego, H. Rebecq, L. Kneip, H. Li, and D. Scaramuzza, "Semi-dense 3d reconstruction with a stereo event camera," in *Proceedings of the European Conference on Computer Vision (ECCV)*. Springer International Publishing, 2018, pp. 235–251. [Online]. Available: <https://link.springer.com/chapter/10.1007>
- [11] H. Rebecq, G. Gallego, E. Mueggler, and D. Scaramuzza, "EMVS: Event-based multi-view stereo—3D reconstruction with an event camera in real-time," *International Journal of Computer Vision*, vol. 126, no. 12, pp. 1394–1414, 2018. [Online]. Available: <https://link.springer.com/article/10.1007>
- [12] L. Steffen, D. Reichard, J. Weinland, J. Kaiser, A. Roennau, and R. Dillmann, "Neuromorphic stereo vision: A survey of bio-inspired sensors and algorithms," *Frontiers in Neurobotics*, vol. 13, p. 28, 2019. [Online]. Available: <https://www.frontiersin.org/articles/10.3389/fnbot.2019.00028/full>
- [13] A. Tremeau, S. Tominaga, and K. Plataniotis, "Color in image and video processing: most recent trends and future research directions," *EURASIP Journal on Image and Video Processing*, vol. 2008, pp. 1–26, 2008. [Online]. Available: <https://link.springer.com/content/pdf/10.1155/2008/581371.pdf>
- [14] A. Marcireau, S.-H. Ieng, C. Simon-Chane, and R. B. Benosman, "Event-based color segmentation with a high dynamic range sensor," *Frontiers in neuroscience*, vol. 12, p. 135, 2018. [Online]. Available: <https://www.frontiersin.org/articles/10.3389/fnins.2018.00135/pdf>
- [15] C. Li, C. Brandli, R. Berner, H. Liu, M. Yang, S.-C. Liu, and T. Delbruck, "Design of an rgbw color vga rolling and global shutter dynamic and active-pixel vision sensor," in *2015 IEEE International Symposium on Circuits and Systems (ISCAS)*. IEEE, 2015, pp. 718–721. [Online]. Available: <https://ieeexplore.ieee.org/document/7168734>
- [16] G. Taverni, D. P. Moeys, C. Li, C. Cavaco, V. Motsnyi, D. S. S. Bello, and T. Delbruck, "Front and back illuminated dynamic and active pixel vision sensors comparison," *IEEE Transactions on Circuits and Systems II: Express Briefs*, vol. 65, no. 5, pp. 677–681, 2018. [Online]. Available: <https://ieeexplore.ieee.org/document/8334288>
- [17] D. P. Moeys, C. Li, J. N. Martel, S. Bamford, L. Longinotti, V. Motsnyi, D. S. S. Bello, and T. Delbruck, "Color temporal contrast sensitivity in dynamic vision sensors," in *2017 IEEE International Symposium on Circuits and Systems (ISCAS)*. IEEE, 2017, pp. 1–4. [Online]. Available: <https://ieeexplore.ieee.org/document/8050412>
- [18] D. P. Moeys, F. Corradi, C. Li, S. A. Bamford, L. Longinotti, F. F. Voigt, S. Berry, G. Taverni, F. Helmchen, and T. Delbruck, "A sensitive dynamic and active pixel vision sensor for color or neural imaging applications," *IEEE transactions on biomedical circuits and systems*, vol. 12, no. 1, pp. 123–136, 2017. [Online]. Available: <https://ieeexplore.ieee.org/document/8094907>
- [19] C. Brandli, T. Mantel, M. Hutter, M. Höpflinger, R. Berner, R. Siegwart, and T. Delbruck, "Adaptive pulsed laser line extraction for terrain reconstruction using a dynamic vision sensor," *Frontiers in neuroscience*, vol. 7, p. 275, 2014. [Online]. Available: <https://www.frontiersin.org/articles/10.3389/fnins.2013.00275/full>
- [20] N. Matsuda, O. Cossairt, and M. Gupta, "MC3D: Motion Contrast 3D Scanning," in *2015 IEEE International Conference on Computational Photography (ICCP)*. IEEE, 2015, pp. 1–10. [Online]. Available: <https://ieeexplore.ieee.org/document/7168370>
- [21] M. Muglikar, D. P. Moeys, and D. Scaramuzza, "Event guided depth sensing," in *2021 International Conference on 3D Vision (3DV)*. IEEE, 2021, pp. 385–393. [Online]. Available: <https://ieeexplore.ieee.org/document/9665844>
- [22] M. Muglikar, G. Gallego, and D. Scaramuzza, "Esl: Event-based structured light," in *2021 International Conference on 3D Vision (3DV)*. IEEE, 2021, pp. 1165–1174. [Online]. Available: <https://ieeexplore.ieee.org/document/9665929>
- [23] B. E. Bayer, "Color imaging array," *United States Patent 3,971,065*, 1976.
- [24] R. Ramanath, W. E. Snyder, Y. Yoo, and M. S. Drew, "Color image processing pipeline," *IEEE Signal Processing Magazine*, vol. 22, no. 1, pp. 34–43, 2005. [Online]. Available: <https://ieeexplore.ieee.org/document/1407713>
- [25] D. Khashabi, S. Nowozin, J. Jancsary, and A. W. Fitzgibbon, "Joint demosaicing and denoising via learned nonparametric random fields," *IEEE Transactions on Image Processing*, vol. 23, no. 12, pp. 4968–4981, 2014. [Online]. Available: <https://ieeexplore.ieee.org/document/6906294>
- [26] A. Levin, D. Lischinski, and Y. Weiss, "Colorization using optimization," in *ACM SIGGRAPH 2004 Papers*, 2004, pp. 689–694. [Online]. Available: <https://dl.acm.org/doi/10.1145/1186562.1015780>
- [27] R. Zhang, P. Isola, and A. A. Efros, "Colorful image colorization," in *European conference on computer vision*. Springer, 2016, pp.

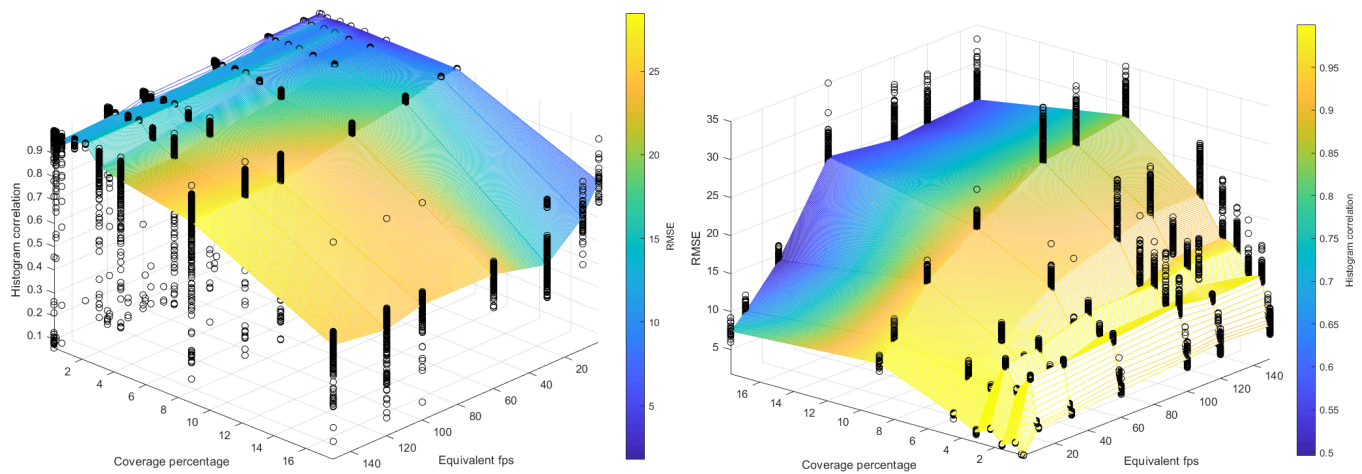


Fig. 13. Comparing patterns with different CPs in speed and quality of the color detection.

- 649–666. [Online]. Available: https://link.springer.com/chapter/10.1007/978-3-319-46487-9_40
- [28] H. W. Jang and Y. J. Jung, “Deep color transfer for color-plus-monocular cameras,” *Sensors*, vol. 20, no. 9, p. 2743, 2020. [Online]. Available: <https://www.mdpi.com/1424-8220/20/9/2743>
- [29] G. Munda, C. Reinbacher, and T. Pock, “Real-time intensity-image reconstruction for event cameras using manifold regularisation,” *International Journal of Computer Vision*, vol. 126, no. 12, pp. 1381–1393, 2018. [Online]. Available: <https://link.springer.com/article/10.1007/s11263-018-1106-2>
- [30] C. Scheerlinck, N. Barnes, and R. Mahony, “Continuous-time intensity estimation using event cameras,” in *Asian Conference on Computer Vision*. Springer, 2018, pp. 308–324. [Online]. Available: https://link.springer.com/chapter/10.1007/978-3-030-20873-8_20
- [31] H. Rebecq, R. Ranftl, V. Koltun, and D. Scaramuzza, “Events-to-video: Bringing modern computer vision to event cameras,” in *Proceedings of the IEEE/CVF Conference on Computer Vision and Pattern Recognition*, 2019, pp. 3857–3866. [Online]. Available: https://openaccess.thecvf.com/content_CVPR_2019/html/Rebecq_Events-To-Video_Bringing_Modern_Computer_Vision_to_Event_Cameras_CVPR_2019_paper.html
- [32] C. Scheerlinck, N. Barnes, and R. Mahony, “Asynchronous spatial image convolutions for event cameras,” *IEEE Robotics and Automation Letters*, vol. 4, no. 2, pp. 816–822, 2019. [Online]. Available: <https://ieeexplore.ieee.org/document/8613800>
- [33] L. Pan, C. Scheerlinck, X. Yu, R. Hartley, M. Liu, and Y. Dai, “Bringing a blurry frame alive at high frame-rate with an event camera,” in *Proceedings of the IEEE/CVF Conference on Computer Vision and Pattern Recognition*, 2019, pp. 6820–6829. [Online]. Available: https://openaccess.thecvf.com/content_CVPR_2019/html/Pan_Bringing_a_Blurry_Frame_Alive_at_High_Frame-Rate_With_an_Event_CVPR_2019_paper.html
- [34] C. Haoyu, T. Minggui, S. Boxin, W. Yizhou, and H. Tiejun, “Learning to deblur and generate high frame rate video with an event camera,” *arXiv preprint arXiv:2003.00847*, 2020. [Online]. Available: <https://arxiv.org/abs/2003.00847>
- [35] N. Messikommer, S. Georgoulis, D. Gehrig, S. Tulyakov, J. Erbach, A. Bochicchio, Y. Li, and D. Scaramuzza, “Multi-bracket high dynamic range imaging with event cameras,” *arXiv preprint arXiv:2203.06622*, 2022. [Online]. Available: <https://arxiv.org/abs/2203.06622>
- [36] H. Rebecq, R. Ranftl, V. Koltun, and D. Scaramuzza, “High speed and high dynamic range video with an event camera,” *IEEE transactions on pattern analysis and machine intelligence*, vol. 43, no. 6, pp. 1964–1980, 2019. [Online]. Available: <https://ieeexplore.ieee.org/document/8946715>
- [37] L. Pan, R. Hartley, C. Scheerlinck, M. Liu, X. Yu, and Y. Dai, “High frame rate video reconstruction based on an event camera,” *IEEE Transactions on Pattern Analysis and Machine Intelligence*, 2020. [Online]. Available: <https://ieeexplore.ieee.org/document/9252186>
- [38] M. Mostafavi, L. Wang, and K.-J. Yoon, “Learning to reconstruct hdr images from events, with applications to depth and flow prediction,” *International Journal of Computer Vision*, vol. 129, no. 4, pp. 900–920, 2021. [Online]. Available: <https://link.springer.com/article/10.1007/s11263-020-01410-2>
- [39] C. Scheerlinck, H. Rebecq, T. Stoffregen, N. Barnes, R. Mahony, and D. Scaramuzza, “Ced: Color event camera dataset,” in *Proceedings of the IEEE/CVF Conference on Computer Vision and Pattern Recognition Workshops*, 2019, pp. 0–0. [Online]. Available: https://openaccess.thecvf.com/content_CVPRW_2019/html/EventVision/Scheerlinck_CED_Color_Event_Camera_Dataset_CVPRW_2019_paper.html
- [40] D. Gehrig and D. Scaramuzza, “Are high-resolution event cameras really needed?” *arXiv preprint arXiv:2203.14672*, 2022. [Online]. Available: <https://arxiv.org/abs/2203.14672>
- [41] S. Muthu, F. J. Schuurmans, and M. D. Pashley, “Red, green, and blue led based white light generation: issues and control,” in *Conference Record of the 2002 IEEE Industry Applications Conference. 37th IAS Annual Meeting (Cat. No. 02CH37344)*, vol. 1. IEEE, 2002, pp. 327–333. [Online]. Available: <https://ieeexplore.ieee.org/document/1044108>
- [42] S. Muthu and J. Gaines, “Red, green and blue led-based white light source: implementation challenges and control design,” in *38th IAS Annual Meeting on Conference Record of the Industry Applications Conference, 2003.*, vol. 1. IEEE, 2003, pp. 515–522. [Online]. Available: <https://ieeexplore.ieee.org/document/1257549>
- [43] A. David and L. A. Whitehead, “Led-based white light,” *Comptes Rendus Physique*, vol. 19, no. 3, pp. 169–181, 2018. [Online]. Available: <https://www.sciencedirect.com/science/article/pii/S163107051830029X>
- [44] M. Pharr, W. Jakob, and G. Humphreys, *Physically based rendering: From theory to implementation*. Morgan Kaufmann, 2016. [Online]. Available: <https://www.sciencedirect.com/book/9780128006450/physically-based-rendering>
- [45] W. Choi, H. S. Park, and C.-M. Kyung, “Color reproduction pipeline for an rgbw color filter array sensor,” *Optics Express*, vol. 28, no. 10, pp. 15 678–15 690, 2020. [Online]. Available: <https://opg.optica.org/oe/fulltext.cfm?uri=oe-28-10-15678&id=431622>
- [46] T. Finateu, A. Niwa, D. Matolin, K. Tsuchimoto, A. Mascheroni, E. Reynaud, P. Mostafalu, F. Brady, L. Chotard, F. LeGoff *et al.*, “5.10 a 1280× 720 back-illuminated stacked temporal contrast event-based vision sensor with 4.86 μm pixels, 1.066 geps readout, programmable event-rate controller and compressive data-formatting pipeline,” in *2020 IEEE International Solid-State Circuits Conference-(ISSCC)*. IEEE, 2020, pp. 112–114. [Online]. Available: <https://ieeexplore.ieee.org/document/9063149>
- [47] T. Delbruck, R. Graca, and M. Paluch, “Feedback control of event cameras,” in *Proceedings of the IEEE/CVF Conference on Computer Vision and Pattern Recognition*, 2021, pp. 1324–1332. [Online]. Available: https://openaccess.thecvf.com/content_CVPR2021W/EventVision/html/Delbruck_Feedback_Control_of_Event_Cameras_CVPRW_2021_paper.html

- [48] H. Levy, "Determining local depth from structured light using a regular dot grid," *Technical Disclosure Commons*, 2019. [Online]. Available: https://www.tdcommons.org/dpubs_series/2536/
- [49] Y. Wang, X. Chen, J. Tao, K. Wang, and M. Ma, "Accurate feature detection for out-of-focus camera calibration," *Applied optics*, vol. 55, no. 28, pp. 7964–7971, 2016. [Online]. Available: <https://opg.optica.org/ao/fulltext.cfm?uri=ao-55-28-7964&id=350405>
- [50] S. Van der Jeught and J. J. Dirckx, "Real-time structured light profilometry: a review," *Optics and Lasers in Engineering*, vol. 87, pp. 18–31, 2016. [Online]. Available: <https://www.sciencedirect.com/science/article/pii/S0143816616000166>
- [51] G. G. Guilbault, *Practical fluorescence*. CRC Press, 2020.
- [52] J. F. Blinn, "Models of light reflection for computer synthesized pictures," in *Proceedings of the 4th annual conference on Computer graphics and interactive techniques*, 1977, pp. 192–198. [Online]. Available: <https://dl.acm.org/doi/abs/10.1145/563858.563893>